

# Mode Coupling and Cavity-Quantum-Dot Interactions in a Fiber-Coupled Microdisk Cavity

Kartik Srinivasan\* and Oskar Painter

Department of Applied Physics, California Institute of Technology, Pasadena, California 91125

(Dated: February 9, 2020)

A quantum master equation model for the interaction between a two-level system and whispering gallery modes (WGMs) of a microdisk cavity is presented, with specific attention paid to current experiments involving a semiconductor quantum dot (QD) embedded in a fiber-coupled, AlGaAs microdisk cavity. In standard single mode cavity QED, three important rates characterize the system: the QD-cavity coupling rate  $g$ , the cavity decay rate  $\kappa$ , and the QD dephasing rate  $\gamma_{\perp}$ . A more accurate model of the microdisk cavity includes two additional features. The first is a second cavity mode that can couple to the QD, which for an ideal microdisk corresponds to a traveling wave WGM propagating counter to the first WGM. The second feature is a coupling between these two traveling wave WGMs, at a rate  $\beta$ , due to backscattering caused by surface roughness that is present in fabricated devices. We consider the transmitted and reflected signals from the cavity for different parameter regimes of  $\{g, \beta, \kappa, \gamma_{\perp}\}$ . A result of this analysis is that even in the presence of negligible roughness-induced backscattering, a strongly coupled QD mediates coupling between the traveling wave WGMs, resulting in an enhanced effective coherent coupling rate  $g = \sqrt{2}g_0$  corresponding to that of a standing wave WGM with electric field maxima at the position of the QD.

PACS numbers:

## I. INTRODUCTION

Recent demonstrations of vacuum Rabi splitting in systems consisting of a semiconductor microcavity and a single quantum dot (QD) [1, 2, 3] represent an important milestone in investigations of cavity QED in solid-state materials. In these experiments, the microcavity-QD system is incoherently pumped with an excitation beam at an energy above the bandgap of both the QD and surrounding semiconductor material (usually GaAs or some form of its alloy AlGaAs). This pump light is absorbed and generates carriers in the GaAs system that can eventually (through phonon and carrier scattering) fill the states of the QD; under weak enough pumping conditions, only the lowest energy bound exciton state of the QD is appreciably populated on average. Radiative recombination of the exciton state and the resulting spontaneous emission is then modified by the presence of a resonant microcavity. When the cavity is of small enough volume, the coupling ( $g$ ) between the QD exciton and the cavity can be large, and if the cavity decay rate  $\kappa$  and QD dephasing rate  $\gamma_{\perp}$  are smaller than  $g$ , the system is said to be strongly coupled [4], in that the QD exciton and cavity mode are no longer truly separate entities but are instead bound together. In the experiments described in refs. [1, 2, 3], the evidence of this strong coupling has been presented in the form of spontaneous emission measurements from the QD-microcavity system, which display a double-peaked structure, rather than the single peak associated with either the cavity mode or QD exciton alone. This vacuum Rabi splitting [5, 6] is one signature of the strong coupling regime in cQED.

Applications of strongly coupled QD-microcavity systems to areas such as nonlinear optics [7, 8, 9, 10, 11] will also require an ability to effectively couple light into and out of the microcavity-QD device. That is, rather than measuring the spontaneous emission of the system alone, it is also important to have access to the cavity's optical response (transmission or reflection). This is true if, for example, one wants to examine the effect of a coupled QD-cavity system on the propagation of a subsequent beam through the cavity [7, 12], or if one wants to use the phase of the emerging transmitted signal within some type of logic gate [13]. Indeed, in most cavity QED experiments involving an atom coupled to a Fabry-Perot cavity, it is the cavity's transmitted or reflected signal that is typically observed [14, 15, 16, 17].

Following demonstrations of coupling to *silica*-based cavities such as microspheres[18, 19] and microtoroids[20], we have recently shown that optical fiber tapers[18, 21] are an effective means to couple light into and out of wavelength-scale, semiconductor microcavities such as photonic crystals[22, 23] and microdisks[24, 25]. In addition, we have shown that microdisk cavities are extremely promising candidates for semiconductor cQED experiments, with recent demonstrations of cavity quality factors ( $Q$ ) in excess of  $10^5$ [25, 26] for devices with a mode volume ( $V_{\text{eff}}$ ) of  $\sim 2 - 6(\lambda/n)^3$ . These  $Q$  values are significantly larger than those utilized in Refs. [1, 2, 3], and as a result, the devices that we consider are poised to operate well within the strong coupling regime, where multiple coherent interactions between the QD and photon can occur. It is envisioned that initial experiments in this fiber-coupled microcavity-QD system will examine vacuum-Rabi splitting through measurements of the

---

\*Electronic address: kartik@caltech.edu

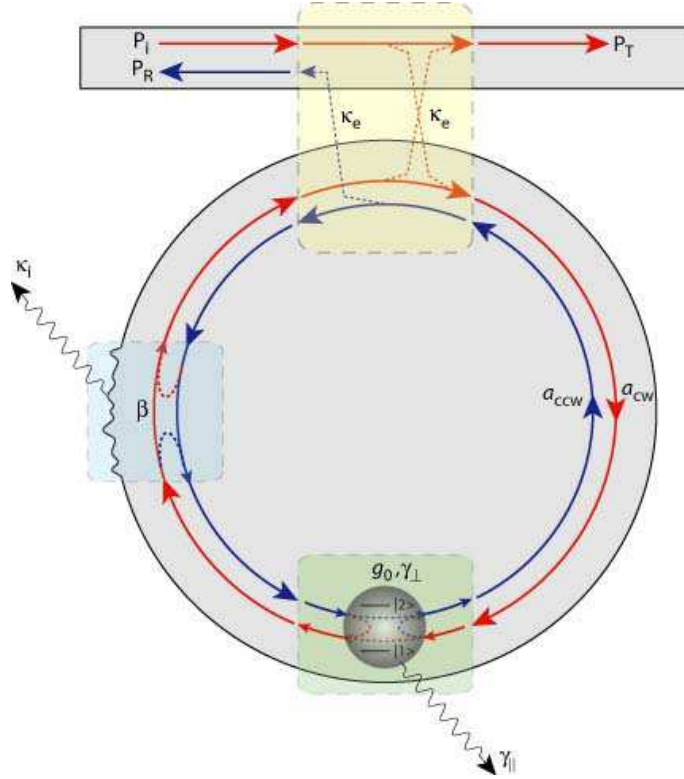


FIG. 1: Illustration of the system under investigation. The microcavity-quantum-dot system is driven near resonance by coupling light into and out of it using an optical fiber taper waveguide, with a cavity-waveguide coupling rate  $\kappa_e$  ( $\kappa_e$  is a *field* amplitude decay rate). Imperfections in the microdisk cause a coupling of the clockwise and counterclockwise whispering gallery modes, at a rate  $\beta$ . These two whispering gallery modes have a quantum-dot-cavity coupling rate  $g_0$  and intrinsic cavity decay rate  $\kappa_i$ . The quantum dot, approximated as a two-level system, has a radiative decay rate  $\gamma_{\parallel}$  and a total transverse decay rate  $\gamma_{\perp}$ .

transmission spectrum past the cavity; such measurements will be directly analogous to recent measurements of vacuum Rabi splitting from one-and-the-same atom in a Fabry-Perot cavity [17].

The goal of this paper is to provide a theoretical basis, accompanied by numerical simulations, for the experiments to be performed with single QDs in fiber-coupled microdisk cavities. Of particular concern is the proper treatment of the whispering gallery modes (WGMs) in the cavities. More specifically, for a given dominant polarization, transverse electric (TE) or transverse magnetic (TM), the WGMs have a degeneracy of two as modes with azimuthal number  $\pm m$  have the same frequency, but circulate around the disk in opposite directions. The WGMs are typically excited through an external waveguide (such as a fiber taper), and for a nearly phase-matched system the forward propagating mode through the waveguide excites only the co-propagating mode in the resonator (the clockwise (*cw*) traveling wave WGM from here on out). Imperfections in the resonator will change this, as they cause backscattering that can couple the *cw* and counterclockwise (*ccw*) propagating modes (Fig. 1) [24, 27, 28, 29, 30]. If the loss rates in the system (due to material absorption, scattering loss, etc.) are low enough, the backscattering can lead to coherent coupling of the *cw* and *ccw* modes, producing a pair of standing wave modes. A similar theoretical model focused on cooled alkali atoms coupled to dielectric whispering-gallery-mode microcavities has been presented by Rosenblit, et al., in Ref. 31, and more recently by Aoki, et al., in Ref. 32. In this work our interest is to study this system in a parameter regime relevant to experiments involving the interaction of a single self-assembled semiconductor quantum dot with the microdisk WGMs in the presence of this backscattering, and to determine the spectral response of the system for varying degrees of quantum-dot-cavity coupling ( $g_0$ ), backscattering ( $\beta$ ), and modal loss ( $\kappa_T$ ). We examine how the phase and magnitude of the backscattering parameter affect the coupling between one or both cavity modes and the QD, and how the QD itself serves to couple the cavity modes together resulting in an enhanced coherent coupling rate over that of traveling wave WGMs.

The organization of this paper is as follows: in section II, we review the simple classical coupled mode theory for modal coupling in microdisk cavities in absence of a QD. Section III presents the quantum mechanical analysis of this system in the presence of a QD. We review the quantum master equation for this system and look at semiclassical approximations for specific choices of the backscattering parameter. In section IV, we present the results of numerical solutions of the quantum master equation for parameters that are accessible in current experiments.

## II. MODAL COUPLING OF TWO WHISPERING GALLERY MODES DUE TO SURFACE SCATTERING

The modal coupling between *cw* and *ccw* traveling wave modes in a whispering-gallery-mode microcavity has been observed experimentally and explained by many other authors, including those of Refs. 24, 27, 28, 29, 33. Here, we present a simple analysis of this coupling. This analysis is essentially an abridged version of that which appears in a recent paper by Borselli, et al., in Ref. 30.

Maxwell's wave equation for the vector electric field in a microdisk structure is

$$\nabla^2 \mathbf{E} - \mu_0 \left( \epsilon^0 + \delta\epsilon \right) \frac{\partial^2 \mathbf{E}}{\partial t^2} = 0, \quad (1)$$

where  $\mu_0$  is the permeability of free space,  $\epsilon^0$  is the dielectric function for the ideal (perfectly circular) microdisk and  $\delta\epsilon$  is the dielectric perturbation that is the source of mode coupling between the *cw* and *ccw* modes. Assuming a harmonic time dependence, the modes of the ideal microdisk structure are  $\mathbf{E}_j^0(\mathbf{r}, t) = \mathbf{E}_j^0(\mathbf{r}) \exp(i\omega_j t)$ , and are solutions of eq. (1) with  $\delta\epsilon = 0$ . Solutions to eq. (1) with  $\delta\epsilon \neq 0$  (i.e., modes of the perturbed structure) are written as a sum of the unperturbed mode basis

$$\mathbf{E}(\mathbf{r}, t) = e^{-i\omega_0 t} \sum_j a_j(t) \mathbf{E}_j^0(\mathbf{r}). \quad (2)$$

Plugging into equation (1), keeping only terms up to first order, and utilizing mode orthogonality, we arrive at the coupled mode equations

$$\frac{da_k}{dt} + i\Delta\omega_k a_k(t) = i \sum_j \beta_{jk} a_j(t) \quad (3)$$

$$\beta_{jk} = \frac{\omega_0}{2} \frac{\int \delta\epsilon(\mathbf{E}_j^0(\mathbf{r}))^* \cdot \mathbf{E}_k^0(\mathbf{r}) d\mathbf{r}}{\int \epsilon^0 |\mathbf{E}_k^0(\mathbf{r})|^2 d\mathbf{r}}. \quad (4)$$

Reference [30] presents a functional form for  $\beta$  in situations involving small surface roughness perturbation. Under weak scattering conditions an assumption is made that only each pair of localized, degenerate *cw* and *ccw* WGMs of azimuthal mode number  $\pm m$  (with dominant polarization (TE or TM) and radial mode number  $p$ ) are coupled by the disk perturbation  $\delta\epsilon$ . The coupled mode equations for these traveling wave modes then read as

$$\begin{aligned} \frac{da_{cw}}{dt} &= -i\Delta\omega a_{cw}(t) + i|\beta| e^{i\xi} a_{ccw}(t) \\ \frac{da_{ccw}}{dt} &= -i\Delta\omega a_{ccw}(t) + i|\beta| e^{-i\xi} a_{cw}(t), \end{aligned} \quad (5)$$

with  $\beta = |\beta| e^{i\xi}$  given by the integral in cylindrical coordinates  $(\phi, \rho, z)$ ,

$$\beta = \frac{\omega_0}{2} \frac{\int (\int e^{+i2m\phi} \delta\epsilon(\phi, \rho, z) d\phi) (\mathbf{E}_{cw}^0(\rho, z))^2 \rho d\rho dz}{\int \epsilon^0 |\mathbf{E}_{cw}^0(\mathbf{r})|^2 d\mathbf{r}}. \quad (6)$$

In order to highlight the dependence of the phase  $\xi$  of the backscattering parameter upon the azimuthal variation of the dielectric perturbation  $\delta\epsilon$  we have substituted the  $e^{\pm im\phi}$  azimuthal field patterns of the traveling wave WGMs into eq. (6).

Equation (5) represents the time evolution of the two mode amplitudes ( $a_{cw}, a_{ccw}$ ) of an isolated system, without loss or coupling to an external waveguide. For the experiments considered in our work, the waveguide coupler will be an optical fiber taper through which light is traveling in the forward propagating mode. Light will then be coupled into the clockwise WGM of the microdisk structure, and this can be included through the addition of the term  $ks$  to equation (5), where  $k$  is a waveguide coupling coefficient and  $|s|^2$  the normalized input *power* (the mode amplitudes  $a_{cw,ccw}$  are normalized to *energy*). Loss is introduced to the coupled mode equations by use of the phenomenological field *amplitude* decay rate  $\kappa_T$ , taken to be the same for both the *cw* and *ccw* modes (though in general this does not have to be the case). This total field decay rate is broken into a contribution from intrinsic microdisk absorption and scattering loss ( $\kappa_i$ ) and a contribution due to coupling to the

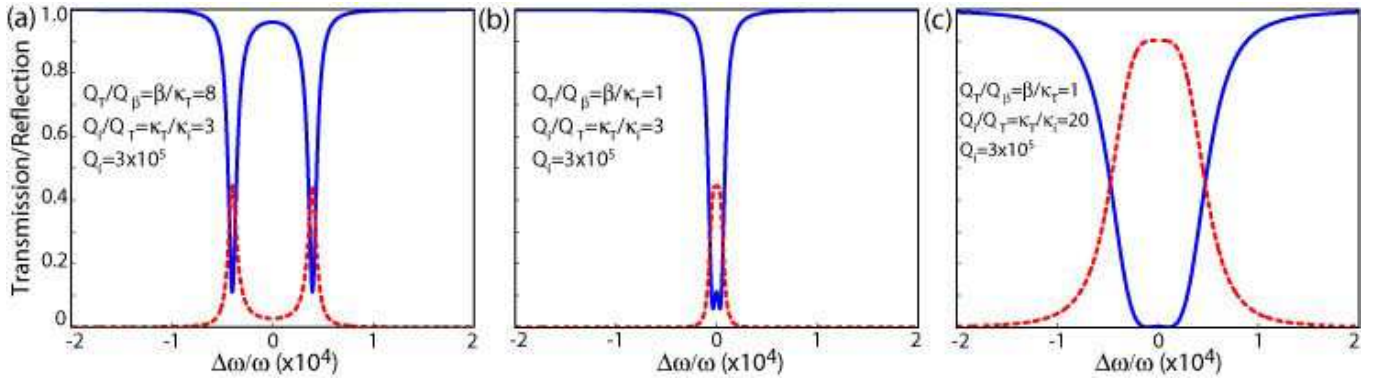


FIG. 2: Normalized transmitted (solid line) and reflected (dashed line) signal for standing wave whispering gallery modes, determined through steady state solution of the coupled mode equations given in equation (7). (a)  $\beta/\kappa_T = 8$ ,  $\kappa_T/\kappa_i = 3$  (b)  $\beta/\kappa_T = 1$ ,  $\kappa_T/\kappa_i = 3$ , and (c)  $\beta/\kappa_T = 1$ ,  $\kappa_T/\kappa_i = 20$ .  $Q_i = 3 \times 10^5$  in all cases.

external waveguide ( $\kappa_e$ ), so that  $\kappa_T = \kappa_i + \kappa_e$ . Assuming lossless coupling and time reversal symmetry, it can be shown [34] that  $|k|^2 = 2\kappa_e$ . The coupled mode equations then read:

$$\begin{aligned} \frac{da_{cw}}{dt} &= -(\kappa_T + i\Delta\omega)a_{cw}(t) + i|\beta|e^{i\xi}a_{ccw}(t) + is\sqrt{2\kappa_e} \\ \frac{da_{ccw}}{dt} &= -(\kappa_T + i\Delta\omega)a_{ccw}(t) + i|\beta|e^{-i\xi}a_{cw}(t), \end{aligned} \quad (7)$$

Here, the phase of the coupling coefficient was (arbitrarily) chosen to be purely imaginary, corresponding to a purely real single-pass transmission coefficient in the lossless coupler case[34]. These two coupled equations can be rewritten as uncoupled equations in terms of the variables  $a_{sw,1}$  and  $a_{sw,2}$ , which represent the standing wave mode amplitudes

$$\begin{aligned} a_{sw,1} &= \frac{1}{\sqrt{2}}(a_{cw} + e^{i\xi}a_{ccw}) \\ a_{sw,2} &= \frac{1}{\sqrt{2}}(a_{cw} - e^{i\xi}a_{ccw}). \end{aligned} \quad (8)$$

As mentioned above, for an ideal microdisk the field distributions of mode amplitudes  $a_{cw}$  and  $a_{ccw}$  have an azimuthal spatial dependence of  $e^{\pm im\phi}$ , so that the field distributions of  $a_{sw,1}$  and  $a_{sw,2}$  correspond to (up to an overall phase factor) standing waves  $\sqrt{2}\cos(m\phi - \xi/2)$  and  $\sqrt{2}\sin(m\phi - \xi/2)$ , respectively, with the azimuthal orientation of the standing waves being determined by the phase  $\xi$  of the backscattering parameter. Here, and in what follows, we take the origin of the azimuthal axis ( $\phi = 0$ ) to be centered at the QD.

The transmitted ( $P_T$ ) and reflected ( $P_R$ ) optical power in the external waveguide can be determined in either the basis of  $\{a_{cw}, a_{ccw}\}$  or  $\{a_{sw,1}, a_{sw,2}\}$ ; because our formulation of the problem has an external waveguide input  $s$  that is a source for  $a_{cw}$ , it is most natural to solve for these quantities in the traveling wave mode basis, and they are given by  $P_T = | -s - i\sqrt{2\kappa_e}a_{cw}|^2$  and  $P_R = |\sqrt{2\kappa_e}a_{ccw}|^2$ . Steady state solutions for the normalized transmitted and reflected signals from the cavity for a number of different parameters are shown in Fig. 2. For  $\beta > \kappa_T$  (Fig. 2(a)), we see the formation of a distinct pair of resonances, located at  $\omega \approx \omega_0 \pm \beta$ . These dips correspond to standing wave resonances that result from a backscattering rate ( $\beta$ ) that exceeds all other losses in the system ( $\kappa_T$ ) so that coherent coupling between the *cw* and *ccw* modes can take place. As we see in Fig. 2(b)-(c), for  $\beta \sim \kappa_T$ , the resonances begin to overlap and are no longer distinguishable.

For cavity QED applications, one very important consequence of the distinction between traveling wave and standing wave modes is in the effective volume of the mode ( $V_{\text{eff}}$ ), as the peak electric field strength per photon in the cavity scales as  $1/\sqrt{V_{\text{eff}}}$ . In particular, we recall the definition of  $V_{\text{eff}}$  as:

$$V_{\text{eff}} = \frac{\int \epsilon |\mathbf{E}(\mathbf{r})|^2}{\max[\epsilon |\mathbf{E}(\mathbf{r})|^2]}. \quad (9)$$

Standing wave WGMs have approximately half the volume of the traveling wave WGMs, so that the coupling rate  $g$  between a single quantum dot and a single photon in a standing wave cavity mode is expected to be  $\sqrt{2}$  times that when the quantum dot

is coupled to a traveling wave cavity mode. This of course assumes the single QD is positioned at an antinode of the standing wave mode; alternately, if it happens to be positioned at a node, the coupling rate  $g$  will be zero.

These arguments again rely upon having a physical system in which the backscattering coupling between *cw* and *ccw* modes is sufficiently strong compared to all other loss rates to allow for coherent modal coupling to form standing wave modes. They have also assumed that the QD does not introduce loss into the system. This is clearly not the case if the QD is strongly coupled to a cavity mode. In strong coupling, energy oscillates back and forth between the QD and the cavity, so that QD decay terms can also cause loss. In this case, we might expect that standing wave modes can be maintained provided that the modal coupling rate  $\beta$  exceeds not only  $\kappa_T$ , but also the QD spontaneous emission rate  $\gamma_{||}$  and non-radiative dephasing rate  $\gamma_p$ . To verify our physical intuition and understand the system in better detail, we consider a quantum master equation approach [35] to take into account the cavity-QD interaction.

### III. QUANTUM MASTER EQUATION MODEL

We begin by considering the Hamiltonian for an empty microdisk cavity (traveling wave WGM resonance frequency  $\omega_c$ ) with field operators  $\hat{a}_{cw}$  and  $\hat{a}_{ccw}$  and mode coupling parameter  $\beta$ , written in a frame rotating at the driving frequency  $\omega_l$ :

$$H_0 = \Delta\omega_{cl}\hat{a}_{cw}^\dagger\hat{a}_{cw} + \Delta\omega_{cl}\hat{a}_{ccw}^\dagger\hat{a}_{ccw} - \beta\hat{a}_{cw}^\dagger\hat{a}_{ccw} - \beta^*\hat{a}_{ccw}^\dagger\hat{a}_{cw} + i(E\hat{a}_{cw}^\dagger - E^*\hat{a}_{cw}), \quad (10)$$

where  $\Delta\omega_{cl} = \omega_c - \omega_l$ . Here, the *cw* propagating mode is driven by an intracavity field  $E = -i\sqrt{2\kappa_e P_{in}}$ , where  $\kappa_e$  is the cavity field decay rate into the waveguide and  $P_{in}$  is the input power in the external waveguide. In this and all equations that follow, Planck's constant is taken as unity,  $\hbar = 1$ . From this Hamiltonian, the classical coupled-mode equations without dissipation can easily be derived through an application of Ehrenfest's theorem.

Modeling the QD as a two-level system, we add the term  $H_1$  to the Hamiltonian:

$$H_1 = \Delta\omega_{al}\hat{\sigma}_+\hat{\sigma}_- + ig_0(\hat{a}_{cw}^\dagger\hat{\sigma}_- - \hat{a}_{cw}\hat{\sigma}_+) + ig_0(\hat{a}_{ccw}^\dagger\hat{\sigma}_- - \hat{a}_{ccw}\hat{\sigma}_+) \quad (11)$$

where  $\Delta\omega_{al} = \omega_a - \omega_l$ ,  $\omega_a$  is the transition frequency of the excitonic state of the QD, and  $g_0$  is the coherent coupling strength between the QD exciton state and the *traveling wave* WGMs. The equation of motion for the system's density matrix  $\rho$  can then be found from the equation:

$$\frac{d\rho}{dt} = \frac{1}{i}[H_0 + H_1, \rho] + L\rho \quad (12)$$

where the term  $L\rho = (L_1 + L_2 + L_3)\rho$  allows for the inclusion of decay through cavity loss (at a rate  $\kappa_T = \omega_c/2Q$ ), quantum dot spontaneous emission (at a rate  $\gamma_{||}$ ), and phase-destroying collisional processes (at a rate  $\gamma_p$ ), which are of particular importance for quantum dots, as unlike atoms, they are embedded in a semiconductor matrix where electron-phonon scattering is non-negligible. These loss terms are given by [35, 36]:

$$L_1\rho = \kappa_T(2\hat{a}_{cw}\rho\hat{a}_{cw}^\dagger - \hat{a}_{cw}^\dagger\hat{a}_{cw}\rho - \rho\hat{a}_{cw}^\dagger\hat{a}_{cw}) + \kappa_T(2\hat{a}_{ccw}\rho\hat{a}_{ccw}^\dagger - \hat{a}_{ccw}^\dagger\hat{a}_{ccw}\rho - \rho\hat{a}_{ccw}^\dagger\hat{a}_{ccw}) \quad (13)$$

$$L_2\rho = \frac{\gamma_{||}}{2}(2\hat{\sigma}_-\rho\hat{\sigma}_+ - \hat{\sigma}_+\hat{\sigma}_-\rho - \rho\hat{\sigma}_+\hat{\sigma}_-) \quad (14)$$

$$L_3\rho = \frac{\gamma_p}{2}(\hat{\sigma}_z\rho\hat{\sigma}_z - \rho) \quad (15)$$

From this master equation, we can numerically calculate the steady state density matrix  $\rho_{ss}$  and relevant operator expectation values such as  $\langle\hat{a}_{cw}^\dagger\hat{a}_{cw}\rangle_{ss}$ , which will then allow us to determine the transmission and reflection spectrum of the coupled QD-cavity system, using formulas that are analogous to those used in the classical model of section II. These calculations are the subject of the following section. For now, however, we consider what intuition may be gained by further analytical study of the

master equation. We take operator expectation values to arrive at:

$$\begin{aligned}
\frac{d}{dt} \langle \hat{a}_{cw} \rangle &= -i\Delta\omega_{cl} \langle \hat{a}_{cw} \rangle + i\beta \langle \hat{a}_{ccw} \rangle + g_0 \langle \hat{\sigma}_- \rangle - \kappa_T \langle \hat{a}_{cw} \rangle + E \\
\frac{d}{dt} \langle \hat{a}_{ccw} \rangle &= -i\Delta\omega_{cl} \langle \hat{a}_{ccw} \rangle + i\beta^* \langle \hat{a}_{cw} \rangle + g_0 \langle \hat{\sigma}_- \rangle - \kappa_T \langle \hat{a}_{ccw} \rangle \\
\frac{d}{dt} \langle \hat{\sigma}_- \rangle &= -(i\Delta\omega_{al} + \gamma_{\perp}) \langle \hat{\sigma}_- \rangle + g_0 (\langle \hat{\sigma}_z \hat{a}_{cw} \rangle + \langle \hat{\sigma}_z \hat{a}_{ccw} \rangle) \\
\frac{d}{dt} \langle \hat{\sigma}_z \rangle &= -2g_0 (\langle \hat{\sigma}_- \hat{a}_{cw}^\dagger \rangle + \langle \hat{\sigma}_+ \hat{a}_{cw} \rangle) - 2g_0 (\langle \hat{\sigma}_- \hat{a}_{ccw}^\dagger \rangle + \langle \hat{\sigma}_+ \hat{a}_{ccw} \rangle) \\
&\quad - \gamma_{\parallel} (1 + \langle \hat{\sigma}_z \rangle)
\end{aligned} \tag{16}$$

where  $[\hat{\sigma}_+, \hat{\sigma}_-] = \hat{\sigma}_z$  and  $\gamma_{\perp} = \gamma_{\parallel}/2 + \gamma_p$ .

In the semi-classical approximation, where expectation values of products of operators equal the product of the expectation values, and writing  $\beta = |\beta| e^{i\xi}$ , these equations reduce to

$$\begin{aligned}
\frac{d}{dt} \langle \hat{a}_{cw} \rangle &= -i\Delta\omega_{cl} \langle \hat{a}_{cw} \rangle + i|\beta| e^{i\xi} \langle \hat{a}_{ccw} \rangle + g_0 \langle \hat{\sigma}_- \rangle - \kappa_T \langle \hat{a}_{cw} \rangle + E \\
\frac{d}{dt} \langle \hat{a}_{ccw} \rangle &= -i\Delta\omega_{cl} \langle \hat{a}_{ccw} \rangle + i|\beta| e^{-i\xi} \langle \hat{a}_{cw} \rangle + g_0 \langle \hat{\sigma}_- \rangle - \kappa_T \langle \hat{a}_{ccw} \rangle \\
\frac{d}{dt} \langle \hat{\sigma}_- \rangle &= -(i\Delta\omega_{al} + \gamma_{\perp}) \langle \hat{\sigma}_- \rangle + g_0 (\langle \hat{\sigma}_z \rangle \langle \hat{a}_{cw} \rangle + \langle \hat{\sigma}_z \rangle \langle \hat{a}_{ccw} \rangle) \\
\frac{d}{dt} \langle \hat{\sigma}_z \rangle &= -2g_0 \langle \hat{\sigma}_- \rangle (\langle \hat{a}_{cw}^\dagger \rangle + \langle \hat{a}_{ccw}^\dagger \rangle) - 2g_0 \langle \hat{\sigma}_+ \rangle (\langle \hat{a}_{cw} \rangle + \langle \hat{a}_{ccw} \rangle) \\
&\quad - \gamma_{\parallel} (1 + \langle \hat{\sigma}_z \rangle)
\end{aligned} \tag{17}$$

From equation 8 of section II, we expect that the first two equations above can be uncoupled if written in terms of standing wave operators,

$$\begin{aligned}
\hat{a}_{sw,1} &= \frac{1}{\sqrt{2}} (\hat{a}_{cw} + e^{i\xi} \hat{a}_{ccw}) \\
\hat{a}_{sw,2} &= \frac{1}{\sqrt{2}} (\hat{a}_{cw} - e^{i\xi} \hat{a}_{ccw}).
\end{aligned} \tag{18}$$

Re-writing the operator evolution equations in terms of these quantities, we arrive at

$$\begin{aligned}
\frac{d}{dt} \langle \hat{a}_{sw,1} \rangle &= -i(\Delta\omega_{cl} - |\beta|) \langle \hat{a}_{sw,1} \rangle + g_0 \frac{1+e^{i\xi}}{\sqrt{2}} \langle \hat{\sigma}_- \rangle - \kappa_T \langle \hat{a}_{sw,1} \rangle + E \\
\frac{d}{dt} \langle \hat{a}_{sw,2} \rangle &= -i(\Delta\omega_{cl} + |\beta|) \langle \hat{a}_{sw,2} \rangle + g_0 \frac{1-e^{i\xi}}{\sqrt{2}} \langle \hat{\sigma}_- \rangle - \kappa_T \langle \hat{a}_{sw,2} \rangle + E \\
\frac{d}{dt} \langle \hat{\sigma}_- \rangle &= -(i\Delta\omega_{al} + \gamma_{\perp}) \langle \hat{\sigma}_- \rangle + \frac{g_0 \langle \hat{\sigma}_z \rangle}{\sqrt{2}} \left( \langle \hat{a}_{sw,1} \rangle (1+e^{-i\xi}) + \langle \hat{a}_{sw,2} \rangle (1-e^{-i\xi}) \right) \\
\frac{d}{dt} \langle \hat{\sigma}_z \rangle &= -\sqrt{2}g_0 \langle \hat{\sigma}_- \rangle \left( \langle \hat{a}_{sw,1}^\dagger \rangle (1+e^{i\xi}) + \langle \hat{a}_{sw,2}^\dagger \rangle (1-e^{i\xi}) \right) \\
&\quad - \sqrt{2}g_0 \langle \hat{\sigma}_+ \rangle \left( \langle \hat{a}_{sw,1} \rangle (1+e^{-i\xi}) + \langle \hat{a}_{sw,2} \rangle (1-e^{-i\xi}) \right) - \gamma_{\parallel} (1 + \langle \hat{\sigma}_z \rangle).
\end{aligned} \tag{19}$$

These equations indicate that, in this basis, we have a modified QD-cavity coupling strength for each standing wave mode, which have shifted in frequency in comparison to the traveling wave modes and are now centered at  $\omega_c \mp |\beta|$ . For the first mode, corresponding to field operator  $\hat{a}_{sw,1}$ , the effective coupling strength is  $g_{sw,1} = g_0(1+e^{i\xi})/\sqrt{2}$ , while for the second mode, corresponding to field operator  $\hat{a}_{sw,2}$ , the effective coupling strength is  $g_{sw,2} = g_0(1-e^{i\xi})/\sqrt{2}$ . These coupling strengths are thus dependent on the phase  $\xi$  of the backscattering parameter  $\beta$ ; they can be as large as  $\sqrt{2}g_0$  and as small as zero. This result is consistent with what we would expect based upon the physical intuition that the superposition of traveling wave modes will result in a pair of standing wave modes whose volume  $V_{\text{eff}}$  is one-half that of the traveling wave modes. The two modes are

phase shifted from each other in the azimuthal direction by  $\pi/2$ , and as a result, if the QD is positioned in the antinode of one mode ( $\xi=0$ , so that  $g_{sw,1}=\sqrt{2}g_0$ ), it is within a node of the other mode (so that  $g_{sw,2}=0$ ), and vice versa for the situation when  $\xi=\pi$ .

The semiclassical equations can be solved in steady state to yield information about the cavity response as a function of drive strength and detunings. In the case of a single cavity mode coupled to a two-level system this leads to the standard optical bistability state equation (OBSE) [37, 38]. Such a semiclassical solution might be of increased importance in the current work because of the potentially large system size that needs to be considered in the numerical simulations of the quantum master equation, due to the presence of two cavity modes. This will be particularly true when considering relatively large driving fields, which could be of interest in nonlinear spectroscopy of the system, for example, as in Ref. 39. For now, we consider a couple of simple examples, beginning with the case of  $\xi=0$  (the  $\xi=\pi$  case is identical except the roles of  $\hat{a}_{sw,1}$  and  $\hat{a}_{sw,2}$  are swapped). Defining the following parameters:

$$\begin{aligned} n_s &= \frac{\gamma_{\perp}\gamma_{\parallel}}{4g_0^2}, \\ C &= \frac{g_0^2}{2\kappa T\gamma_{\perp}}, \\ Y &= \frac{E}{\kappa T}n_s^{-1/2}, \\ X_{sw,1} &= \langle\hat{a}_{sw,1}\rangle n_s^{-1/2}, \\ X_{sw,2} &= \langle\hat{a}_{sw,2}\rangle n_s^{-1/2}, \end{aligned} \tag{20}$$

we solve (in steady state) the semiclassical equations of motion in the standing wave basis (eq. (19)) to arrive at the following expression:

$$\begin{aligned} X_{sw,1} &= \frac{Y}{1 + \frac{4\sqrt{2}C}{2X_{sw,1}^2 + \left(\frac{\Delta\omega_{al}}{\gamma_{\perp}}\right)^2 + 1} + i\left(\frac{\sqrt{2}(\Delta\omega_{cl}-\beta)}{\kappa} - \frac{4\sqrt{2}C\left(\frac{\Delta\omega_{al}}{\gamma_{\perp}}\right)}{2X_{sw,1}^2 + \left(\frac{\Delta\omega_{al}}{\gamma_{\perp}}\right)^2 + 1}\right)} \\ X_{sw,2} &= \frac{Y}{1 + i\left(\frac{\Delta\omega_{cl}+\beta}{\kappa}\right)} \end{aligned} \tag{21}$$

We are most interested in obtaining an expression for the optical transmission (or reflection) past the cavity and into our collection fiber, which will be the quantity measured in experiment. In the formalism presented in section II, the transmission and reflection are given in terms of the traveling wave mode operators. These operators can easily be recovered here from odd and even parity superpositions of  $X_{sw,1}$  and  $X_{sw,2}$  (cf eq. (18)).

In the general case both WGMs will couple to the QD and obtaining an equation analogous to the OBSE for an arbitrary  $\xi$  is somewhat algebraically tedious. As a simple example in which both traveling wave modes are coupled to the QD we consider  $\xi=\pi/2$ , which yields in steady-state:

$$\begin{aligned} Y &= \sqrt{2}X_+ \frac{|\beta|}{\kappa} + \frac{\sqrt{2}X_+}{1 + \frac{|\beta|/\kappa}{1 + i\frac{\Delta\omega_{cl}}{\kappa}}} \left[ \left(1 - \frac{|\beta|}{\kappa} + \frac{4C}{2X_+^2 + \left(\frac{\Delta\omega_{al}}{\gamma_{\perp}}\right)^2 + 1}\right) + i\left(\frac{\Delta\omega_{cl}}{\kappa} - \frac{4C\left(\frac{\Delta\omega_{al}}{\gamma_{\perp}}\right)}{2X_+^2 + \left(\frac{\Delta\omega_{al}}{\gamma_{\perp}}\right)^2 + 1}\right) \right] \\ X_- &= \frac{\frac{|\beta|}{\kappa}X_+ + Y/\sqrt{2}}{1 + i\frac{\Delta\omega_{cl}}{\kappa}} \end{aligned} \tag{22}$$

where  $X_+ = (\langle\hat{a}_{cw}\rangle + \langle\hat{a}_{ccw}\rangle)n_s^{-1/2}$  and  $X_- = (\langle\hat{a}_{cw}\rangle - \langle\hat{a}_{ccw}\rangle)n_s^{-1/2}$ . From  $X_+$  and  $X_-$ ,  $\langle\hat{a}_{cw}\rangle$  and  $\langle\hat{a}_{ccw}\rangle$  can easily be found, and the transmitted and reflected signals from the cavity calculated.

#### IV. SOLUTIONS TO THE STEADY STATE QUANTUM MASTER EQUATION IN THE WEAK DRIVING REGIME

The quantum master equation (QME) presented in the previous section is solved numerically using the Quantum Optics Toolbox [40, 41] for Matlab. We begin by considering steady state solutions, and calculate the transmitted and reflected signals

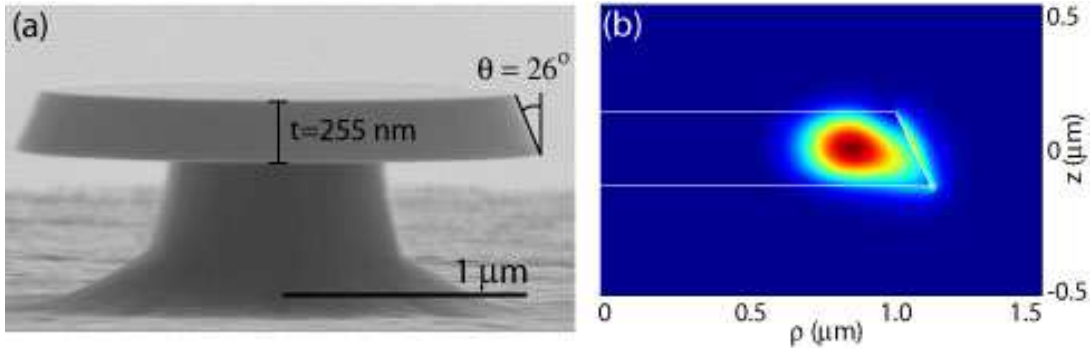


FIG. 3: (a) Scanning electron microscope (SEM) image of a fabricated microdisk device. The disk thickness is  $t=255$  nm and the sidewall angle is  $\theta = 26^\circ$  from vertical. The measured average diameter for this device (i.e., the diameter at the center of the slab) is  $\sim 2.12$   $\mu\text{m}$ . (b) Finite-element-calculated  $|\mathbf{E}|^2$  distribution for the  $\text{TE}_{p=1,m=11}$  WGM of a microdisk with a diameter of  $\sim 2.12$   $\mu\text{m}$  at the center of the slab. For this mode,  $\lambda \sim 1265.41$  nm,  $Q_{\text{rad}} \sim 10^7$ , and for a traveling wave (standing wave) mode,  $V_{\text{eff}} \sim 5.6(\lambda/n)^3$  ( $2.8(\lambda/n)^3$ ).

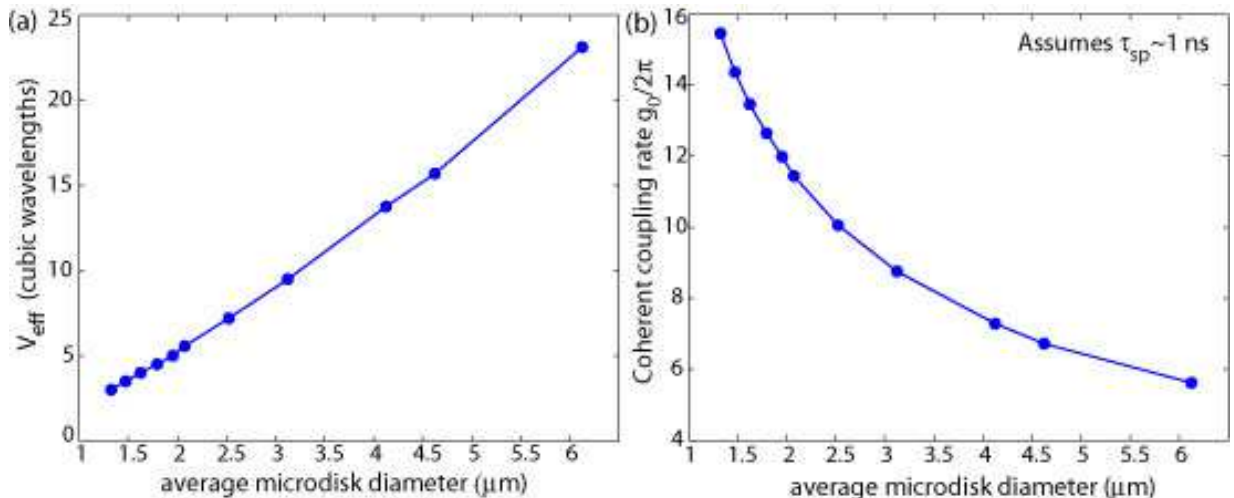


FIG. 4: Finite-element method simulation results: (a) Modal volume  $V_{\text{eff}}$  as a function of microdisk diameter (taken at the center of the slab), calculated for traveling wave modes. The modes studied are  $\text{TE}_{p=1,m}$  WGMs with resonance wavelength within the 1200 nm band. (b) Coherent coupling rate  $g_0/2\pi$  as a function of microdisk diameter. A QD spontaneous emission lifetime  $\tau_{\text{sp}} = 1$  ns is assumed in the calculation of  $g_0$ .

from the cavity in the weak driving regime. As a starting point, we eliminate the quantum dot from the problem by taking the coupling rate  $g_0 = 0$ . As expected, the resulting solutions (not displayed here) are identical to those obtained using the classical coupled mode equations and presented in Fig. 2. Having confirmed that the QME solution is consistent with the classical solution in the empty cavity limit, we move on to study interactions with the quantum dot. To connect these simulations to ongoing experiments, we choose physical parameters consistent with our fabricated devices [25, 26]. In these experiments, the microdisk cavity is 255 nm thick, and has a sidewall angle of  $\sim 26^\circ$ , as shown in Figure 3(a). The modes of these structures (Fig. 3(b)) can be numerically investigated through finite-element eigenfrequency calculations using the Comsol FEMLAB software [26, 42, 43], and information about the effective modal volume  $V_{\text{eff}}$  (as defined in Eqn. 9) and radiation-limited quality factor  $Q_{\text{rad}}$  can be obtained. For the purposes of this work, we focus on modes of transverse electric (TE) polarization, where the electric field lies predominantly within the plane of the disk, and we consider first order radial modes ( $p=1$ ) in the 1200 nm band, the wavelength region of interest in our experiments.

In Fig. 4(a), we plot the calculated  $V_{\text{eff}}$  for traveling wave modes as a function of the average microdisk diameter  $D_{\text{avg}}$ . From

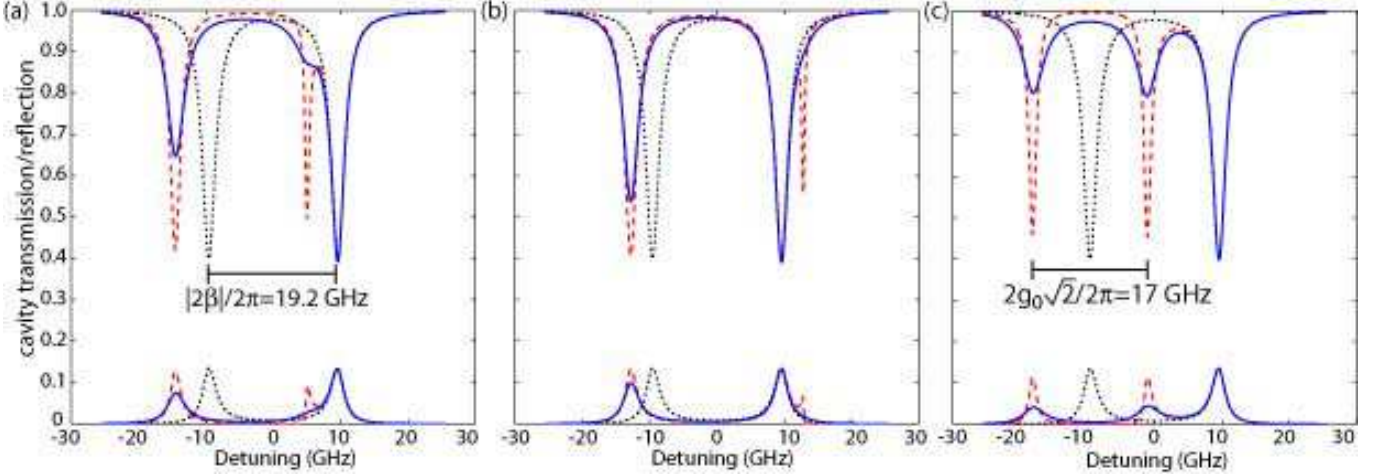


FIG. 5: Normalized transmitted signal (top curves) and reflected signal (bottom curves) for a QD coupled to a microdisk cavity, calculated through numerical solution of the steady state quantum master equation under weak driving. For all of the calculations  $\{g_0, \beta, \kappa_T, \kappa_e, \gamma_{\parallel}, \gamma_p\}/2\pi = \{6, 9.6, 1.2, 0.44, 0.16, 2.4\}$  GHz, with the phase of the backscattering parameter  $\xi = 0$ . (a)  $\Delta\omega_{ac} = \omega_a - \omega_c = 0$ , (b)  $\Delta\omega_{ac} = \beta$ , and (c)  $\Delta\omega_{ac} = -\beta$ , where  $\omega_c$  is the resonance frequency of the traveling wave whispering gallery modes and  $\omega_a$  is the QD exciton transition frequency. In these plots the additional black dotted lines correspond to an empty cavity ( $g_0 = 0$ ) and the red dashed lines correspond to a QD with no non-radiative dephasing  $\gamma_p/2\pi = 0$  GHz.

these values for  $V_{\text{eff}}$  we can calculate the maximum QD-photon coupling strength  $g_0 = \mathbf{d} \cdot \mathbf{E}/\hbar$ , given by [4, 44]:

$$g_0 = \frac{1}{2\tau_{\text{sp}}} \sqrt{\frac{3c\lambda_0^2\tau_{\text{sp}}}{2\pi n^3 V_{\text{eff}}}}, \quad (23)$$

where  $\tau_{\text{sp}}$  is the spontaneous emission lifetime of the QD exciton, which we take as 1 ns in our calculations, consistent with what has been seen experimentally [45]. The results are plotted in Fig. 4(b), and we see that  $g_0/2\pi$  can be as high as 16 GHz for the range of diameters we consider. As discussed in ref. [26], for such modes  $Q_{\text{rad}} > 10^5$  for all but the smallest diameter disks ( $D_{\text{avg}} < 1.5 \mu\text{m}$ ). We have confirmed this in experiments, with  $Q$  as high as  $3.6 \times 10^5$  measured, so that cavity decay rates  $\kappa_T/2\pi$  on the order of 1 GHz can reasonably be expected. Such devices exhibited doublet splittings that were on the order of 10-100 pm, corresponding to a backscattering rate  $|\beta|/2\pi = 1\text{-}10$  GHz. In practical devices then, the roughness-induced backscattering and the coherent QD-cavity mode coupling rates can be of similar magnitude, and we thus expect the simulation results to be particularly helpful in interpreting future experimental data.

### A. $\beta > g_0 > (\kappa_T, \gamma_{\perp})$

The first situation we study is one in which the backscattering rate  $\beta$  exceeds the coupling rate  $g_0$ , which in turn exceeds the cavity and QD decay rates  $\kappa_T$  and  $\gamma_{\perp}$ . We choose  $\beta/2\pi = 9.6$  GHz ( $\xi = 0$ ), with  $g_0/2\pi = 6$  GHz,  $\kappa_T/2\pi = 1.2$  GHz (corresponding to  $Q = 10^5$ ),  $\kappa_e/2\pi = 0.44$  GHz (corresponding to a transmission depth of 60% for the empty-cavity standing wave modes), and  $\tau_{\text{sp}} = 1$  ns ( $\gamma_{\parallel}/2\pi \sim 0.16$  GHz). The unperturbed cavity frequency (i.e., the resonance frequency of the *traveling wave* modes) is fixed at  $\omega_c = 0$ , and three different QD-cavity detunings,  $\Delta\omega_{ac} = \omega_a - \omega_c = \{0, \beta, -\beta\}$  are considered. For each value of  $\Delta\omega_{ac}$ , we calculate the steady state transmission and reflection spectra (as a function of laser-cavity detuning,  $\Delta\omega_{lc}$ ) from the cavity in three different limits: (i)  $g_0 = 0$ ; here, there is no QD-cavity coupling, and the response should be that of an empty cavity, (ii)  $g_0/2\pi = 6$  GHz,  $\gamma_p/2\pi = 0$  GHz; here, we neglect all non-radiative dephasing, which becomes a good approximation as the temperature of the QD is cooled below 10 K, and (iii)  $g_0/2\pi = 6$  GHz,  $\gamma_p/2\pi = 2.4$  GHz; here, we allow for a significant amount of non-radiative dephasing, corresponding to a QD exciton linewidth of  $\sim 10 \mu\text{eV}$ , which is consistent with what has been observed experimentally at temperatures of around 10-20 K [45].

The results of the steady-state quantum master equation simulations are plotted in Fig. 5. The interpretation of these results is as follows: as a result of the modal coupling due to backscattering, which has formed standing wave modes through a superposition of the initial traveling wave modes, only the lower frequency mode of the doublet has any spatial overlap with the QD (see Fig. 6 for location of the QD relative to the two standing wave modes as a function of  $\xi$ ), and thus, we should only

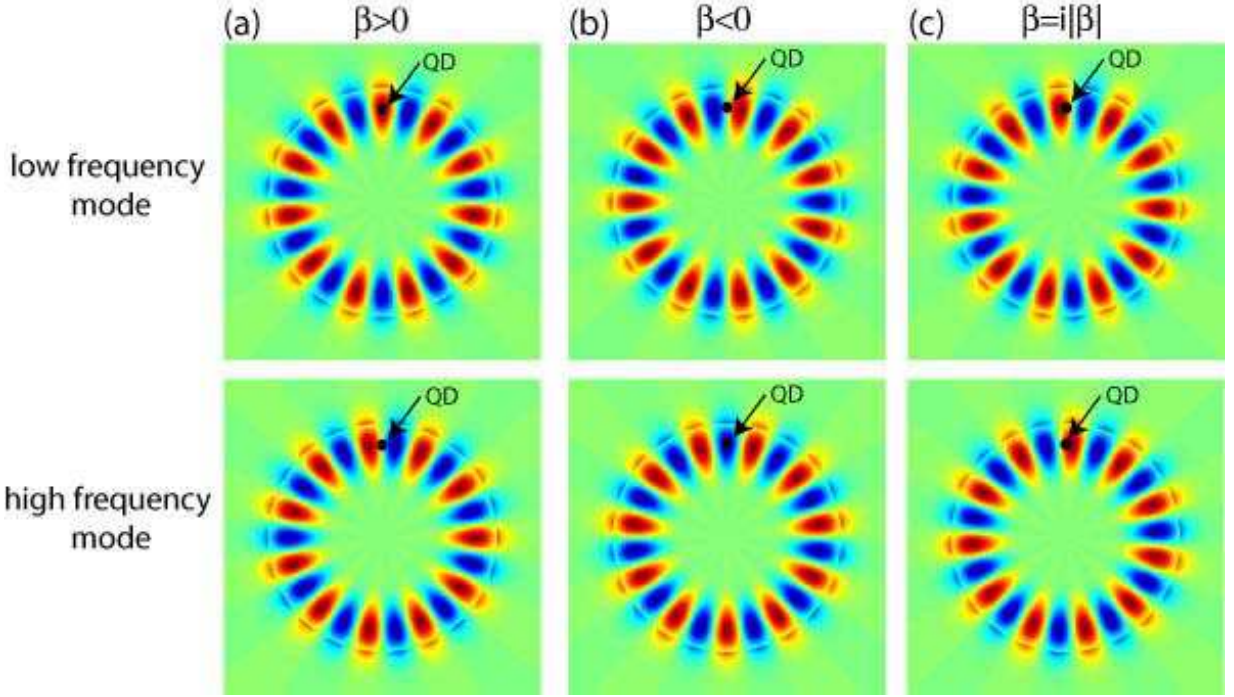


FIG. 6: Standing wave modes in a microdisk for different choices of  $\beta$ , showing how the low and high frequency modes are positioned with respect to a fixed QD. (a)  $\beta > 0$  ( $\xi = 0$ ), (b)  $\beta < 0$  ( $\xi = \pi$ ), and (c)  $\beta = i|\beta|$  ( $\xi = \pi/2$ ).

expect the low frequency mode to exhibit any frequency shifts or splittings. In Fig. 5(a), with the QD spectrally detuned equally from both empty-cavity standing wave modes, we see *asymmetric* vacuum Rabi splitting due to coupling of the QD to the low frequency mode at  $\omega_c - \beta$ . In Fig. 5(b), with the QD now on resonance with the higher frequency mode, coupling still only occurs to the low frequency mode detuned in this case by  $2\beta$ . Finally in Fig. 5(c), the QD is on resonance with the low frequency mode, and is also spatially aligned with it, so that we see the familiar *symmetric* vacuum Rabi splitting of this resonance. We note that the frequency splitting,  $\Omega_R$ , is in this case  $2g_0\sqrt{2}$  rather than  $2g_0$ ; this is consistent with the mode volume of the standing wave modes being one half that of the traveling wave modes, as  $g \sim 1/\sqrt{V_{\text{eff}}}$ . For  $\xi = \pi$  (Fig. 7) the results are the mirror image of those in Fig. 5, where now the high frequency mode is spatially aligned with the QD and exhibits frequency shifts and vacuum Rabi splitting.

Finally, we consider an intermediate backscattering phase  $\xi = \pi/2$ . Here, we expect both modes to have an equal (but non-optimal) spatial alignment with the QD (Fig. 6(c)). The results, displayed in Fig. 8, show that this is indeed the case. In Fig. 8(a), for example, we see a symmetric spectrum, consistent with both modes being equally spatially coupled to the QD and equally (and oppositely) spectrally detuned from it. In Fig. 8(b)-(c), we see that the spectra are no longer symmetric, as the QD is on resonance with the high frequency mode in Fig. 8(b), and with the low frequency mode in Fig. 8(c). In each case we see Rabi splitting about the mode on resonance with the QD and only a small shift for the detuned mode. The Rabi splitting between the peaks is no longer at the maximum value of  $2g_0\sqrt{2}$ , but at a value closer to  $2g_0$  due to the spatial misalignment of the QD with the empty-cavity standing wave modes.

### B. $g_0 > \beta > (\kappa_T, \gamma_{\perp})$

Here we switch regimes slightly to one in which the QD-cavity coupling rate dominates all other rates in the system, including the backscattering rate  $\beta$ . In particular, we choose  $g_0/2\pi=12$  GHz, with  $\beta/2\pi=4.8$  GHz,  $\kappa_T/2\pi=1.2$  GHz ( $\kappa_e/2\pi=0.44$  GHz), and  $\tau_{\text{sp}}=1$  ns ( $\gamma_{\parallel}/2\pi \sim 0.16$  GHz). The qualitative behavior that we expect to see is identical to that of the previous section, as both  $g_0$  and  $\beta$  represent coherent processes, so that their relative values compared to each other are not as important as their values in comparison to the dissipative rates in the system. This is seen in Fig. 9(a), where the QD is spectrally located at  $-\beta$ , so that it is resonant with the low frequency mode of the standing wave doublet. Predictably, the interaction with the QD causes this resonance to split, with a splitting  $\Omega_R=2g_0\sqrt{2}$ . The higher frequency mode remains unaffected, as the choice of  $\xi=0$  causes it to be spatially misaligned from the QD.

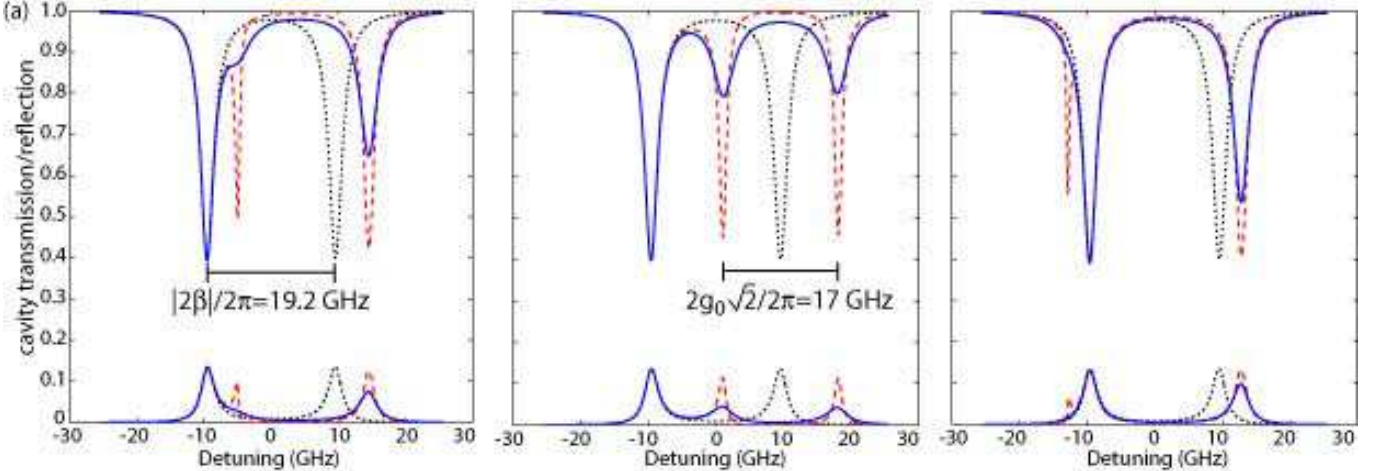


FIG. 7: Normalized transmitted signal (top curves) and reflected signal (bottom curves) for a QD coupled to a microdisk cavity, calculated through numerical solution of the steady state quantum master equation under weak driving. These plots are calculated using identical parameters as those used in Fig. 5, with the exception that the phase of the backscattering parameter  $\beta$  has been changed from  $\xi=0$  to  $\xi=\pi$ , so that  $\beta/2\pi=-9.6$  GHz.

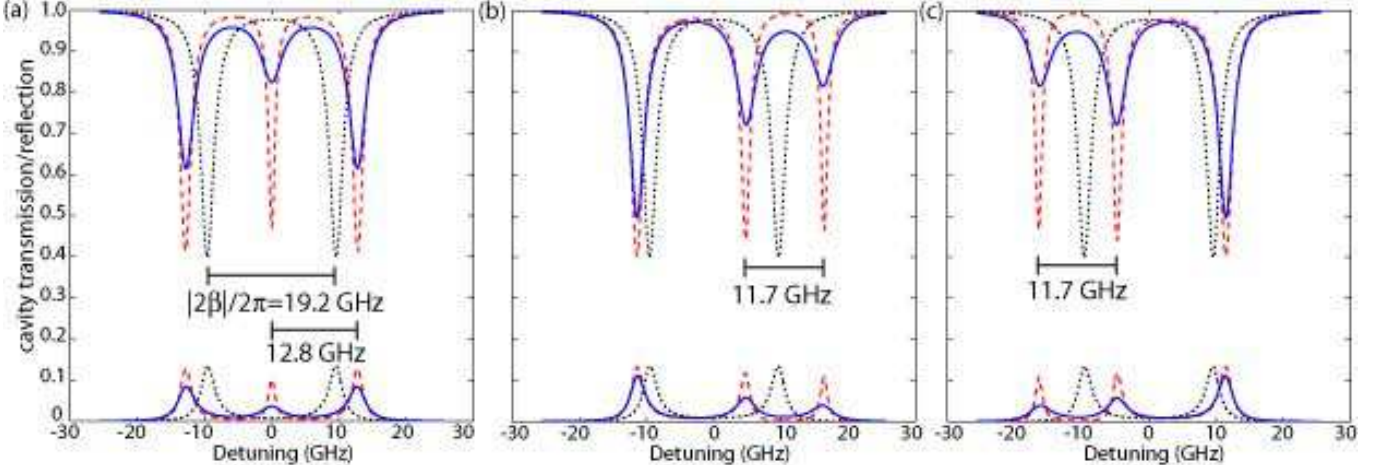


FIG. 8: Normalized transmitted signal (top curves) and reflected signal (bottom curves) for a QD coupled to a microdisk cavity, calculated through numerical solution of the steady state quantum master equation under weak driving. These plots are calculated using identical parameters as those used in Fig. 5, with the exception that the phase of the backscattering parameter  $\beta$  has been changed from  $\xi=0$  to  $\xi=\pi/2$ , so that  $\beta/2\pi=i9.6$  GHz.

### C. $\kappa_T > g_0 > \beta > \gamma_{\perp}$

Now, we take the cavity loss rate  $\kappa_T/2\pi=9.6$  GHz to exceed both  $g_0/2\pi=6$  GHz and  $\beta/2\pi=1.2$  GHz. In addition,  $\kappa_e/2\pi = 3.5$  GHz,  $\gamma_{\parallel}/2\pi=0.16$  GHz, and  $\gamma_p/2\pi=0$  or  $0.7$  GHz, so that  $\kappa_T > \kappa_e > \gamma_{\perp}$  (good cavity limit). In the absence of a QD we expect to see a single transmission dip rather than a doublet for  $\kappa_T \gg \beta$ . This is confirmed in simulation by the black dotted line in Fig. 9(b). With the addition of a QD, taken to be resonant with the center frequency of the single cavity transmission dip, we expect to see this single dip split into two, with the dips not being completely resolved due to decay of the cavity mode ( $\kappa_T > g$ ). This is confirmed in Fig. 9(b), where the splitting  $\Omega_R/2\pi = 14.8$  GHz lies between the expected splitting for a purely traveling wave cavity mode ( $\Omega_R=2g_0$ ) and the expected splitting for a purely standing wave cavity mode ( $\Omega_R=2g_0\sqrt{2}$ ), and lies closer to the former due to the large degree to which  $\kappa_T$  exceeds  $\beta$ .

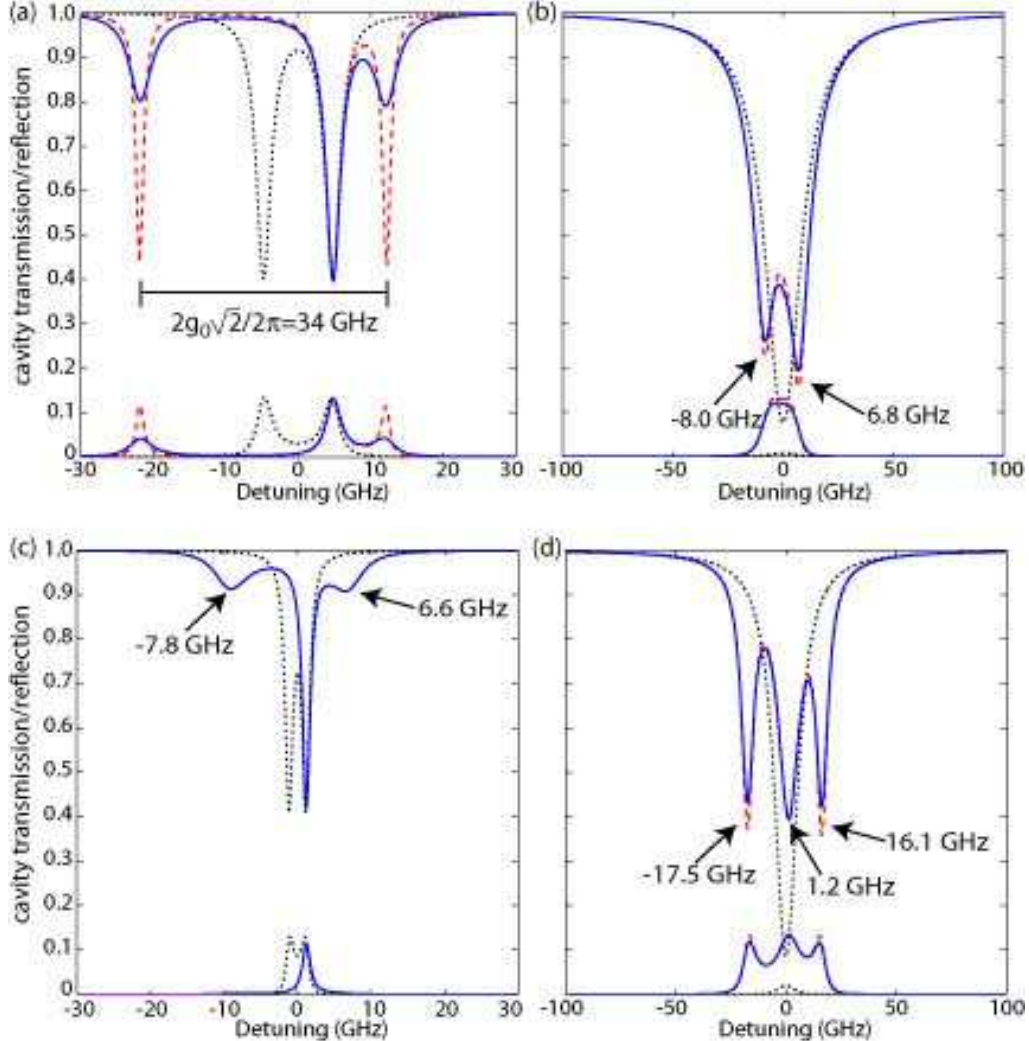


FIG. 9: Normalized transmitted signal (top curves) and reflected signal (bottom curves) for a QD coupled to a microdisk cavity with  $\xi = 0$ , calculated through numerical solution of the steady state quantum master equation under weak driving. (a)  $\kappa_T > g_0 > \beta > \gamma_{\perp}$  ( $\Delta\omega_{ac} = -\beta/2\pi$ ,  $\{g_0, \beta, \kappa_T, \kappa_e, \gamma_{\parallel}, \gamma_p\}/2\pi = \{12, 4.8, 1.2, 0.44, 0.16, 2.4\}$  GHz), (b)  $\kappa_T > g_0 > \beta > \gamma_{\perp}$  ( $\Delta\omega_{ac} = 0$ ,  $\{g_0, \beta, \kappa_T, \kappa_e, \gamma_{\parallel}, \gamma_p\}/2\pi = \{6, 1.2, 9.6, 3.5, 0.16, 0.7\}$  GHz), (c)  $\gamma_{\parallel} > g_0 > \beta > \kappa_T$  ( $\Delta\omega_{ac} = -\beta/2\pi$ ,  $\{g_0, \beta, \kappa_T, \kappa_e, \gamma_{\parallel}, \gamma_p\}/2\pi = \{6, 1.2, 0.6, 0.22, 9.4, 0\}$  GHz), and (d)  $g_0 > \kappa_T > \beta > \gamma_{\perp}$  ( $\Delta\omega_{ac} = 0$ ,  $\{g_0, \beta, \kappa_T, \kappa_e, \gamma_{\parallel}, \gamma_p\}/2\pi = \{12, 1.2, 6, 2.2, 0.16, 0.7\}$  GHz). In these plots the additional black dotted lines correspond to an empty cavity ( $g_0 = 0$ ) and the red dashed lines correspond to a QD with no non-radiative dephasing  $\gamma_p/2\pi = 0$  GHz.

#### D. $\gamma_{\parallel} > g_0 > \beta > \kappa_T$

Here, the roles of  $\kappa_T$  and  $\gamma_{\parallel}$  are swapped in comparison to the previous subsection, so that  $\gamma_{\parallel}/2\pi = 9.6$  GHz is the dominant dissipative rate, exceeding each of  $\{g_0, \beta, \kappa_T, \kappa_e\}/2\pi = \{6, 1.2, 0.6, 0.22\}$  GHz (bad cavity limit). Unlike our previous example, in absence of a QD we do expect to see a pair of standing wave modes form, as  $\beta > \kappa_T$ . This is confirmed in Fig. 9(c) (black dashed line). Now, we introduce a QD that is spectrally aligned with the low frequency mode at  $-\beta$ . Because QD decay is so large in this case we expect that the standing wave character of the modes is going to largely be erased when coupled to the QD. To confirm this intuition, we examine the calculated transmission spectrum in Fig. 9(c). The low frequency mode does indeed split, but the splitting  $\Omega_R/2\pi = 14.4$  GHz is much less than the expected splitting of  $2g_0\sqrt{2}$  for standing wave modes, and lies much closer to the  $2g_0$  splitting for traveling wave modes. The situation thus mimics that of the previous example, although in this case the relatively weak transmission contrast of the QD-coupled resonances is a result of operation in the bad cavity limit.

### E. $g_0 > \kappa_T > \beta > \gamma_{\perp}$

Finally, we consider a scenario in which the QD-cavity coupling  $g_0/2\pi = 12$  GHz is the dominant rate in the system, but where cavity decay  $\kappa_T/2\pi = 6$  GHz exceeds the backscattering rate  $\beta/2\pi = 1.2$  GHz. In absence of a QD we see a single transmission resonance dip (Fig. 9(d)) as  $\kappa_T > \beta$ . If a QD is now spectrally aligned to the center of this transmission dip ( $\Delta\omega_{ac}=0$ ) three resonances appear within the transmission spectrum of Fig. 9(d). This should be contrasted with the transmission spectrum of Fig. 9(b) in which only two resonant transmission dips were present. The central resonance dip of Fig. 9(d) is at a detuned frequency of 1.2 GHz ( $= \beta/2\pi$ ), and corresponds to the frequency of one of the two standing wave modes that can form through an appropriate combination of the traveling wave modes. As this mode is spatially misaligned from the QD for  $\xi = 0$ , we do not expect its frequency to have shifted due to interaction with the QD. The other two transmission resonances correspond to the splitting of the low frequency mode from its empty-cavity position at  $-\beta/2\pi = -1.2$  GHz. The splitting of  $\Omega_R/2\pi = 33.6$  GHz is very close to the value of  $2g_0\sqrt{2}$  expected for interaction with a standing wave mode.

The basic result that the above example demonstrates is that the QD can effectively serve as a means to couple the traveling wave microdisk modes, even in instances where the backscatter parameter is small relative to other rates in the system. As a final illustration of this, we consider the situation where the backscatter parameter is zero. In Fig. 10, the empty-cavity single transmission resonance separates into three resonance dips, one at the original zero detuning and the other two split by  $2g_0\sqrt{2}$ . The interpretation of this result is that the QD has effectively served to couple the two counter-propagating traveling wave modes, creating a pair of standing wave resonant modes, one which is decoupled and has an electric field node at the position of the QD, and the other which is strongly coupled to the QD at a field antinode. In this case, and in other strong coupling cases where  $g_0$  is the dominant system rate, the QD serves to set the position of the effective standing wave cavity modes (as opposed to backscattering phase  $\xi$ ) thus ensuring azimuthal alignment of the QD with a field antinode of one of the standing wave modes. Note that in the example of Sec. IV A (Fig. 5) in which  $\beta > g_0$ , it is the phase of  $\beta$  ( $\xi$ ) which determines the position of the standing wave field antinodes with respect to the QD.

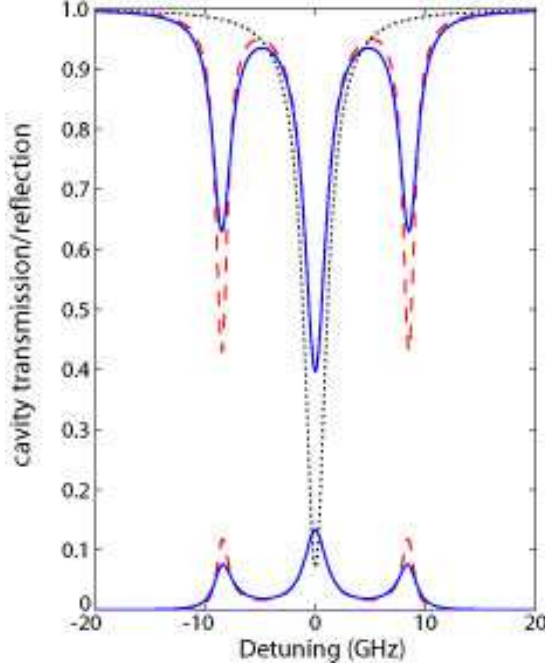


FIG. 10: Normalized transmitted signal (top curves) and reflected signal (bottom curves), for the case where the roughness-induced backscattering rate ( $\beta$ ) is zero.  $g_0 > \kappa_T > \gamma_{\perp} > \beta$  ( $\Delta\omega_{ac} = 0$ ,  $\{g_0, \beta, \kappa_T, \kappa_e, \gamma_{\parallel}, \gamma_p\}/2\pi = \{6, 0, 1.2, 0.44, 0.16, 0.7\}$  GHz). The additional black dotted lines correspond to an empty cavity ( $g_0 = 0$ ) and the red dashed lines correspond to a QD with no non-radiative dephasing  $\gamma_p/2\pi = 0$  GHz.

## V. SUMMARY

We have extended the standard quantum master equation model for a two-level system coupled to the mode of an electromagnetic cavity to better reflect the situation that occurs in studies of microdisk cavities containing an embedded quantum dot. In

particular, the quantum dot, still treated as a two-level system, is coupled to two cavity modes, corresponding to clockwise and counterclockwise counter-propagating whispering gallery modes of the disk. These two modes are in turn passively coupled to each other through surface roughness, characterized by a backscatter parameter  $\beta$ . We examine the steady state behavior of the system for differing regimes of  $\beta$ , the QD-cavity coupling rate  $g_0$ , the cavity decay rate  $\kappa_T$ , and the quantum dot dephasing rate  $\gamma_\perp$ . In particular, we consider conditions for which standing wave cavity modes form, how the magnitude of the different system rates and the phase of  $\beta$  determine the nodes and antinodes of the cavity modes with respect to the quantum dot, and the resulting QD-cavity coupling. It is anticipated that this analysis will be useful in the interpretation of experimental spectra from a waveguide-coupled whispering-gallery mode microcavity strongly coupled to a single two-level system such as the excitonic state of a self-assembled quantum dot.

## VI. ACKNOWLEDGEMENTS

KS thanks the Hertz Foundation for his graduate fellowship support.

---

[1] J. P. Reithmaier, G. Sek, A. Loffer, C. Hoffman, S. Kuhn, S. Reitzenstein, L. V. Keldysh, V. D. Kulakovskii, T. L. Reinecke, and A. Forchel, *Nature* **432**, 197 (2004).

[2] T. Yoshie, A. Scherer, J. Hendrickson, G. Khitrova, H. Gibbs, G. Rupper, C. Ell, Q. Schenkin, and D. Deppe, *Nature* **432**, 200 (2004).

[3] E. Peter, P. Senellart, D. Martrou, A. Lemaître, J. Hours, J. M. Gérard, and J. Bloch, *Phys. Rev. Lett.* **95** (2005).

[4] H. J. Kimble, *Physica Scripta* **T76**, 127 (1998).

[5] J. J. Sanchez-Mondragon, N. B. Narozhny, and J. H. Eberly, *Phys. Rev. Lett.* **51**, 550 (1983).

[6] G. S. Agarwal, *Phys. Rev. Lett.* **53**, 1732 (1984).

[7] Q. A. Turchette, C. J. Hood, W. Lange, H. Mabuchi, and H. J. Kimble, *Phys. Rev. Lett.* **25**, 4710 (1995).

[8] P. R. Rice and H. J. Carmichael, *IEEE J. Quan. Elec.* **24**, 1351 (1988).

[9] C. M. Savage and H. J. Carmichael, *IEEE J. Quan. Elec.* **24**, 1495 (1988).

[10] P. Alsing and H. J. Carmichael, *Journal of Optics B: Quantum Optics* **3**, 13 (1981).

[11] M. A. Armen and H. Mabuchi, quant-ph/0602170 (2006).

[12] K. M. Birnbaum, A. Boca, R. Miller, A. Boozer, T. E. Northup, and H. J. Kimble, *Nature* **436**, 87 (2005).

[13] L.-M. Duan and H. J. Kimble, *Phys. Rev. Lett.* **92**, 127902 (2004).

[14] R. J. Thompson, G. Rempe, and H. J. Kimble, *Phys. Rev. Lett.* **68**, 1132 (1992).

[15] C. J. Hood, T. W. Lynn, A. C. Doherty, A. S. Parkins, and H. J. Kimble, *Science* **287**, 1447 (2000).

[16] P. W. H. Pineske, T. Fischer, P. Maunz, and G. Rempe, *Nature* **404**, 365 (2000).

[17] A. Boca, R. Miller, K. M. Birnbaum, A. D. Boozer, J. McKeever, and H. J. Kimble, *Phys. Rev. Lett.* **93**, 233603 (2004).

[18] J. C. Knight, G. Cheung, F. Jacques, and T. A. Birks, *Opt. Lett.* **22**, 1129 (1997).

[19] M. Cai, O. Painter, and K. J. Vahala, *Phys. Rev. Lett.* **85**, 74 (2000).

[20] D. K. Armani, T. J. Kippenberg, S. M. Spillane, and K. J. Vahala, *Nature* **421**, 925 (2003).

[21] T. A. Birks and Y. W. Li, *J. Lightwave Tech.* **10**, 432 (1992).

[22] K. Srinivasan, P. E. Barclay, M. Borselli, and O. Painter, *Phys. Rev. B* **70**, 081306R (2004).

[23] P. E. Barclay, K. Srinivasan, and O. Painter, *Opt. Express* **13**, 801 (2005).

[24] M. Borselli, K. Srinivasan, P. E. Barclay, and O. Painter, *Appl. Phys. Lett.* **85**, 3693 (2004).

[25] K. Srinivasan, M. Borselli, T. J. Johnson, P. E. Barclay, O. Painter, A. Stintz, and S. Krishna, *Appl. Phys. Lett.* **86**, 151106 (2005).

[26] K. Srinivasan, M. Borselli, O. Painter, A. Stintz, and S. Krishna, *Opt. Express* **14**, 1094 (2006).

[27] D. S. Weiss, V. Sandoghdar, J. Hare, V. Lefèvre-Seguin, J.-M. Raimond, and S. Haroche, *Opt. Lett.* **20**, 1835 (1995).

[28] B. E. Little and S. T. Chu, *Opt. Lett.* **21**, 1390 (1996).

[29] T. J. Kippenberg, S. M. Spillane, and K. J. Vahala, *Opt. Lett.* **27**, 1669 (2002).

[30] M. Borselli, T. J. Johnson, and O. Painter, *Opt. Express* **13**, 1515 (2005).

[31] M. Rosenblit, P. Horak, S. Helsby, and R. Folman, *Phys. Rev. A* **70**, 053808 (2004).

[32] T. Aoki, B. Dayan, E. Wilcut, W. P. Bowen, A. S. Parkins, H. J. Kimble, T. J. Kippenberg, and K. J. Vahala (2006), quant-ph/0606033.

[33] M. L. Gorodetsky, A. D. Pryamikov, and V. S. Ilchenko, *J. Opt. Soc. Am. B* **17**, 1051 (2000).

[34] H. A. Haus, *Waves and Fields in Optoelectronics* (Prentice-Hall, Englewood Cliffs, New Jersey, 1984), 1st ed.

[35] H. J. Carmichael, *An Open Systems Approach to Quantum Optics* (Springer-Verlag, Berlin, 1993).

[36] H. J. Carmichael, *Statistical Methods in Quantum Optics I: Master Equations and Fokker-Planck Equations* (Springer-Verlag, Berlin, 2003).

[37] L. A. Lugiato, *Progress in Optics* **21**, 69 (1984).

[38] H. J. Kimble, *Structure and Dynamics in Cavity Quantum Electrodynamics* (Academic Press, Boston, 1994), pp. 203–266.

[39] R. J. Thompson, Q. A. Turchette, O. Painter, and H. J. Kimble, *Phys. Rev. A* **57**, 3084 (1998).

[40] S. M. Tan, <http://www.qo.phy.auckland.ac.nz/qotoolbox.html> (2002).

[41] S. M. Tan, *Journal of Optics B: Quantum and Semiclassical Optics* **1**, 424 (1999).

[42] S. M. Spillane, T. J. Kippenberg, K. J. Vahala, K. W. Goh, E. Wilcut, and H. J. Kimble, *Phys. Rev. A* **71**, 013817 (2005).

- [43] M. Borselli, T. J. Johnson, and O. Painter, *Appl. Phys. Lett.* **88**, 13114 (2006).
- [44] L. C. Andreani, G. Panzarini, and J.-M. Gérard, *Phys. Rev. B* **60**, 13276 (1999).
- [45] M. Bayer and A. Forchel, *Phys. Rev. B* **65**, 041308(R) (2002).